Weierstraß-Institut
für Angewandte Analysis und Stochastik

im Forschungsverbund Berlin e.V.

Preprint ISSN 0946 – 8633

Dynamics of two mutually coupled semiconductor lasers: instantaneous coupling limit.

Serhiy Yanchuk[1], Klaus R. Schneider[2], Lutz Recke[3]

submitted: October 27, 2003

[1] Weierstrass Institute
for Applied Analysis
and Stochastics
Mohrenstra"se 39
D – 10117 Berlin
Germany
E-Mail: yanchuk@wias-berlin.de

[2] Weierstrass Institute
for Applied Analysis
and Stochastics
Mohrenstra"se 39
D – 10117 Berlin
Germany
E-Mail: schneide@wias-berlin.de

[3] Humboldt-University of Berlin
Institute of Mathematics
Unter den Linden 6
D – 10099 Berlin
Germany
E-Mail: recke@mathematik.hu-berlin.de

No. 879
Berlin 2003

2000 *Mathematics Subject Classification.* 34C15, 34C11, 34C14, 34K20, 34K60, 34C60.

Key words and phrases. two coupled lasers, complete synchronization, antisynchronization, detuning.

Edited by
Weierstraß-Institut für Angewandte Analysis und Stochastik (WIAS)
Mohrenstraße 39
D — 10117 Berlin
Germany

Fax: + 49 30 2044975
E-Mail: preprint@wias-berlin.de
World Wide Web: http://www.wias-berlin.de/

Abstract

We consider two semiconductor lasers coupled face to face under the assumption that the delay time of the injection is small. The model under consideration consists of two coupled rate equations, which approximate the coupled Lang-Kobayashi system as the delay becomes small. We perform a detailed study of the synchronized and antisynchronized solutions for the case of identical systems and compare results from two models: with the delay and with instantaneous coupling. The bifurcation analysis of systems with detuning reveals that self-pulsations appear via bifurcations of stationary (i.e. continuous wave) solutions. We discover the connection between stationary solutions in systems with detuning and synchronous (also antisynchronous) solutions of coupled identical systems. We also identify a codimension two bifurcation point as an organizing center for the emergence of chaotic behavior.

1 Introduction

The goal of the present paper is to study nonlinear dynamics of two mutually coupled semiconductor lasers. We consider the face to face configuration, i.e. the output of each laser is injected into the other laser. The study of such coupling setup is motivated among other facts by the perspective of using masked signal transmission [1, 2]. There is also a hope that such models can provide an additional understanding of the dynamics of two-section laser devices [3]. In addition to the application perspectives for the specific devices, models for coupled lasers turn out to be sources for new physical phenomena such as anticipated or lag synchronization, and chaos appearance for already weak coupling since the isolated lasers operate in a stable stationary regime. From the general perspective of coupled nonlinear oscillators [4], coupled semiconductor lasers usually are modeled by coupled systems with additional symmetry properties which have to be taken into account. Moreover, the significant difference between carrier and photon lifetimes brings multiscale properties into the models.

The dynamics of mutually coupled lasers with large injection feedback time (corresponding to distances from about 10 cm between the lasers) was studied recently in [5, 6, 7]. The case of unidirectional coupling was investigated in [8, 9]. Various new phenomena were reported such as retarded or anticipated synchronization [10, 11, 12, 13], inverse synchronization [14], and antisynchronization of power drop-outs [15].

Recently, there has been appeared new interest in lasers with a short cavity [16], which is motivated by several arguments: First, the study of the dynamics in this regime has become experimentally accessible. Also, such a regime is very interesting from the dynamical point of view, since it has an intermediate complexity, allowing to analyze directly the

mechanisms of either synchronization or the appearance of pulsations and chaotic dynamics. The same arguments seem to be applicable when the delay in the coupling is small, i.e. there is a *short external cavity*. For instance, this is the case in a two-section integrated device [3], where both lasers are parts of the same device and are close to each other *a priori*. The instantaneous coupling limit may serve as an appropriate starting point for the study of such systems. Of course, the smallness of the delay, which allows one to neglect it, is a separate question. From the more general perspective it is still an open problem of modeling: what kind of phenomena in the coupled face to face lasers can be described at least qualitatively by instantaneously coupled rate equations?

It is the main purpose of the present paper to give a comprehensive description of the dynamical regimes arising in a model of instantaneously coupled rate equations. Even neglecting time delay of the injection, it turns out to be important to take into account its relative phase shift φ. For the case of identical lasers, we provide analytical conditions for the stability of synchronized and antisynchronized regimes, where the injection phase shift is the key parameter to determine the dynamics. Similar calculations are compared for two models: the model with small delay and that with instantaneous coupling. Further, we consider the case when there is a detuning between two lasers. It is shown how the injection phase affects the existence and stability of continuous wave solutions and of self-pulsations. It follows that one of the organizing centers for chaotic dynamics is a codimension two Zero-Hopf bifurcation point.

2 The model

The model, which is extensively used to describe the dynamics of mutually coupled single-mode lasers (cf. [5, 9, 8, 17]) is the system of coupled rate equations:

$$\begin{aligned}
\frac{dE_1}{dt} &= i\bar{\delta}E_1 + \frac{1}{2}\left(\mathcal{G}_1(N_1,|E_1|^2) - \frac{1}{\tau_{p_1}}\right)E_1 + \kappa e^{-i\varphi}E_2(t-\bar{\tau}),\\
\frac{dN_1}{dt} &= I_1 - \frac{N_1}{\tau_{c_1}} - \mathrm{Re}[\mathcal{G}_1(N_1,|E_1|^2)]\cdot|E_1|^2,\\
\frac{dE_2}{dt} &= \frac{1}{2}\left(\mathcal{G}_2(N_2,|E_2|^2) - \frac{1}{\tau_{p_2}}\right)E_2 + \kappa e^{-i\varphi}E_1(t-\bar{\tau}),\\
\frac{dN_2}{dt} &= I_2 - \frac{N_2}{\tau_{c_2}} - \mathrm{Re}[\mathcal{G}_2(N_2,|E_2|^2)]\cdot|E_2|^2,
\end{aligned} \tag{1}$$

where $E_{1,2}$ and $N_{1,2}$ denote the complex optical fields and the carrier densities of the lasers, respectively. The term $i\bar{\delta}E_1$ accounts for the frequency detuning. By $I_{1,2}$ we denote the pumping current, and $\mathcal{G}_{1,2}(N_{1,2},|E_{1,2}|^2)$ is the complex gain function. $\tau_{p_{1,2}}$, $\tau_{c_{1,2}}$ are photon and carrier lifetimes; κ and τ characterize the injection rate and the injection delay-time, respectively.

In system (1), we introduce the following simplifications and rescalings. First of all, we assume that all parameters for both lasers are the same except the detuning parameter $\bar{\delta}$. Neglecting nonlinear gain saturation we linearize the complex gain function as follows

$$\mathcal{G}(N,|E|^2) - \frac{1}{\tau_p} := G_N(1+i\alpha)(N-N_0).$$

With the rescaling $E_{\rm new} = \sqrt{G_N \tau_c} E$, $N_{\rm new} = \frac{1}{2}\tau_p G_N (N - N_0)$, $t_{\rm new} = t/\tau_p$ we obtain from (1)

$$\begin{aligned} E_1' &= i\delta E_1 + (1 + i\alpha) N_1 E_1 + \eta e^{-i\varphi} E_2(t - \tau), \\ N_1' &= \varepsilon[J - N_1 - (N_1 + \nu)|E_1|^2], \\ E_2' &= (1 + i\alpha) N_2 E_2 + \eta e^{-i\varphi} E_1(t - \tau), \\ N_2' &= \varepsilon[J - N_2 - (N_2 + \nu)|E_2|^2], \end{aligned} \tag{2}$$

where we use the same notations for the new variables. The differentiation is assumed to be made with respect to the new time, and the parameters are

$$\eta = \tau_p \kappa, \quad \varepsilon = \tau_p/\tau_c, \quad J = \tau_p G_N (I\tau_c - N_0)/2, \quad \tau = \bar{\tau}/\tau_p, \quad \nu = 0.5, \quad \delta = \bar{\delta}\tau_p.$$

In the case $\tau = 0$, we obtain the coupled rate equations with instantaneous coupling:

$$\begin{aligned} E_1' &= i\delta E_1 + (1 + i\alpha) N_1 E_1 + \eta e^{-i\varphi} E_2, \\ N_1' &= \varepsilon[J - N_1 - (N_1 + \nu)|E_1|^2], \\ E_2' &= (1 + i\alpha) N_2 E_2 + \eta e^{-i\varphi} E_1, \\ N_2' &= \varepsilon[J - N_2 - (N_2 + \nu)|E_2|^2]. \end{aligned} \tag{3}$$

System (3) is the main object of this study. In Sec. 7 we compare some of the obtained results with the model (2) which includes small delay.

3 Symmetries. Synchronous and antisynchronous solutions.

Let us first examine the model (3) without detuning, i.e. $\delta = 0$, and note some properties due to inherent symmetries:

$$\begin{aligned} E_j' &= (1 + i\alpha) N_j E_j + \eta e^{-i\varphi} E_{3-j}, \\ N_j' &= \varepsilon[J - N_j - (N_j + \nu)|E_j|^2], \quad j = 1, 2. \end{aligned} \tag{4}$$

1. Since the subsystems are identical, there is a symmetry with respect to indexes interchange $(E_1, N_1, E_2, N_2) \to (E_2, N_2, E_1, N_1)$. This implies the existence of the invariant subspace of synchronous states $E_1 = E_2$ and $N_1 = N_2$.

2. The symmetry $(E_1, N_1, E_2, N_2) \to (-E_2, N_2, E_1, N_1)$ implies the existence of the invariant subspace of antisynchronous states $E_1 = -E_2$ and $N_1 = N_2$.

3. The following symmetry allows us to establish a one-to-one correspondence between synchronous and antisynchronous solutions. If $(E_1(t), N_1(t), E_2(t), N_2(t))$ is a solution to (4) then $(E_1(t), N_1(t), -E_2(t), N_2(t))$ is also a solution provided φ is replaced by $\varphi + \pi$. In other words, the symmetry transformation is of the form $(E_1(t), N_1(t), E_2(t), N_2(t), \varphi) \to (E_1(t), N_1(t), -E_2(t), N_2(t), \varphi + \pi)$. This implies that all antisynchronous solutions and their properties can be obtained from the corresponding synchronous solutions and their properties, which have to be considered for the same parameter values except that φ is shifted by π.

Let us remark, that the coupling, which is present in (4), influences the dynamics in the synchronization and antisynchronization subspaces. This, in particular, makes our situation different from the setup in [4, 18].

4. The phase-shift invariance $(E_1, N_1, E_2, N_2) \to (E_1 e^{i\psi}, N_1, E_2 e^{i\psi}, N_2)$ is common to optical devices without phase conjugation, and, in particular, to the system (2) for any parameter δ and η. This symmetry implies, that for suitable laser parameters there exist continuous wave (CW) solutions, i.e. solutions of the type $E_j(t) = E_{0_j} e^{i\omega t}, N_j = N_{0_j}$ $(j = 1, 2; \omega \in R)$. These solutions are also called "stationary", because they correspond to stationary intensity regimes. Moreover, this symmetry implies that for suitable laser parameters there exist modulated wave (MW) solutions, i.e. solutions of the type $E_j(t) = E_{0_j}(t) e^{i\omega t}, N_j = N_{0_j}(t)$ with $E_{0_j}(t+T) = E_{0_j}(t)$ and $N_{0_j}(t+T) = N_{0_j}(t)$ for all $t \in R$ $(j = 1, 2;\ \omega, T \in R)$. These solutions are also called "periodic" or "self-pulsations", because they correspond to time-periodic intensity regimes.

4 Synchronous CW solutions and their stability

4.1 Dynamics in the synchronization subspace

After substituting $N_1 = N_2 := N$ and $E_1 = E_2 := E$ into (4), we obtain the following equations for the dynamics in the synchronization subspace

$$\begin{aligned} E' &= (1 + i\alpha) N E + \eta e^{-i\varphi} E \\ N' &= \varepsilon [J - N - (N + \nu)|E|^2]. \end{aligned} \tag{5}$$

A qualitative analysis of (5) with $\varepsilon > 0$ and $\nu > 0$ yields the following:

- For $\eta \cos\varphi < -J$ the "off state" $E = 0$, $N = J$ is asymptotically stable.
- For $-J < \eta \cos\varphi < \nu$, there exists a globally stable CW solution $E(t) = E_0 e^{i\omega_0 t}$, $N(t) = N_0$ with

$$\omega_0 = -\eta(\cos\varphi + \sin\varphi), \quad N_0 = -\eta\cos\varphi, \quad E_0 = (J + \eta\cos\varphi)/(\nu - \eta\cos\varphi).$$

Summarizing, let us note that for all physically relevant parameter values, i.e. $J > 0$, $\varepsilon > 0$, $0 < \eta < \nu = 0.5$, there exists a unique stable CW solution inside the synchronization subspace (synchronous CW solution). The same is true for the antisynchronization subspace.

4.2 Transverse stability of the synchronous CW solutions

Since the synchronous CW solution is stable within the synchronization subspace, its stability in the whole phase space is determined by its *transverse* stability, i.e. the stability with respect to perturbations transverse to the synchronization subspace. The analysis of

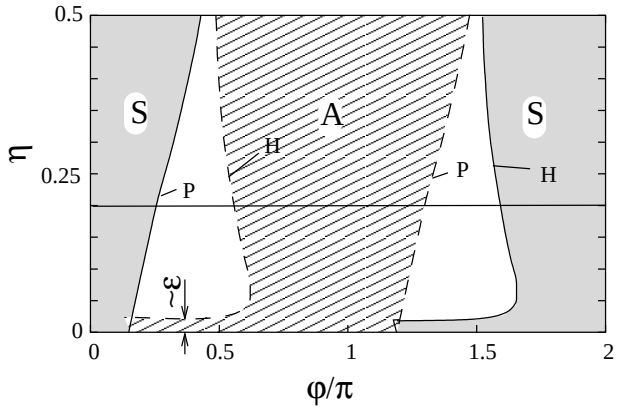

Figure 1: Region of transverse stability for synchronous 'S' and antisynchronous 'A' CW solutions, respectively. 'P' denotes the curves of transverse pitchfork bifurcations and 'H' Hopf bifurcations for the parameters $\alpha = 2$, $J = 1$, $\varepsilon = 0.03$.

the transverse stability of synchronous CW solutions can be carried out by inspecting the characteristic equation

$$\begin{aligned} \chi_T^0(\Lambda) &= \left[\Lambda^2 + 4\Lambda\eta\cos\varphi + 4\eta^2\right](\Lambda + \varepsilon(1+S_0)) \\ &\quad +2\varepsilon S_0(\nu - \eta\cos\varphi)\left[\Lambda + 2\eta(\cos\varphi - \alpha\sin\varphi)\right] = 0, \end{aligned} \tag{6}$$

where

$$S_0 := \frac{J - \eta\cos\varphi}{\nu + \eta\cos\varphi}.$$

This equation is derived in Appendix A. We shall note that the roots of $\chi_T^0(\Lambda) = 0$ determine only transverse stability of the synchronous CW solutions, since the general characteristic equation can be factorized into two equations one of which corresponding to transverse directions and another to the directions within the synchronization subspace, cf. App. A. Transverse pitchfork bifurcation takes place if there is a zero eigenvalue, i.e. $\chi_T^0(0) = 0$, and transverse Hopf bifurcation corresponds to the existence of pure imaginary eigenvalues, i.e. $\chi_T^0(i\Omega) = 0$, where $\Omega \neq 0$ is some real parameter. These bifurcations can be identified and path-followed with respect to the system parameters. Here we choose the coupling strength η and injection phase φ to be the key parameters with respect to which we want to study the dynamics. Typical bifurcation diagram is shown in Figure 1. The figure shows regions for transverse stability of the synchronous CW solution (marked by 'S') and antisynchronous CW solution (marked by 'A'), respectively. Note that in order to obtain the result for antisynchronous solutions, we used the symmetry arguments of Sec. 3, i.e. the region 'A' is an image of the region 'S', which is shifted by π along the parameter axis φ. The transverse bifurcations that mediate the loss of synchronization are marked as 'P' for pitchfork and 'H' for Hopf, respectively. Note that we do not show in Fig. 1 all the bifurcation lines, but only those which mediate the stability loss of CW solutions.

There are also small regions where stable synchronous and stable antisynchronous CW solutions coexist. They are located at $\varphi = \arctan(1/\alpha)$ and $\varphi = \arctan(1/\alpha) + \pi$ and their size is of order ε, cf. Fig 2.

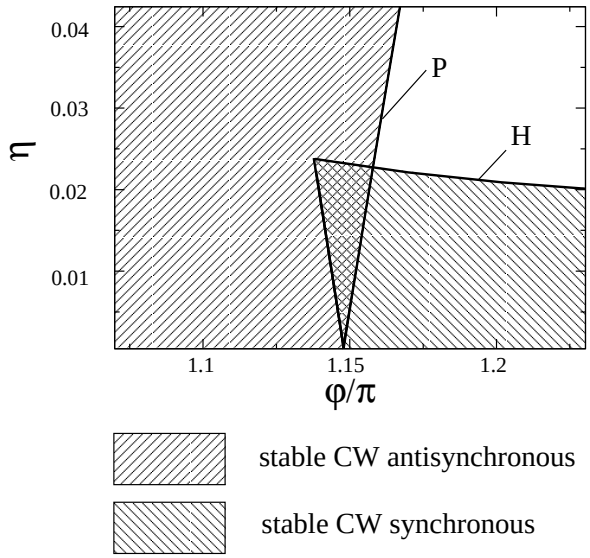

Figure 2: Zoom of the small part of Fig. 1. The regions of stability of synchronous and antisynchronous CW solutions are overlapped, creating multistability. Here the bifurcation curves are shown completely, i.e. not only those parts that bounds the stability regions of the corresponding CW solutions.

The bifurcation diagrams, cf. Figs. 1-2, also reveals that the first destabilization threshold, i.e. destabilization of the CW solutions with increasing of the coupling η for fixed ϕ, may occur already for coupling strength of order ε via Hopf bifurcation.

5 Asynchronous CW solutions

Synchronous and antisynchronous CW solutions are not the only possible stationary solutions in the system (4). Another set of CW solutions, which we call *asynchronous*, can be obtained from the following anzats:

$$E_1(t) = a_1 e^{i(\omega t+\psi)}, \quad N_1(t) = N_1 = \text{const}, \quad E_2(t) = a_2 e^{i\omega t}, \quad N_2(t) = N_2 = \text{const}, \quad (7)$$

where $a_1, a_2, N_1, N_2, \omega, \psi$ are real constants to be determined. After substituting it into (4), we obtain a set of nonlinear equations, which afterward can be effectively studied numerically. We refer the reader to Appendix B for details. As a result we present the one-dimensional bifurcation diagram in Fig. 3, which corresponds to the parameters as in Fig. 1 but with fixed $\eta = 0.2$ (cf. horizontal line in the figure). In addition to the synchronous and antisynchronous solutions, we observe branches of unstable asynchronous orbits connecting synchronous and antisynchronous CW solutions. These branches emerge from the subcritical pitchfork bifurcations P_s and P_a, respectively. Although these solutions are unstable their role may be important in forming the boundary of the attracting region of stable synchronous CW solutions.

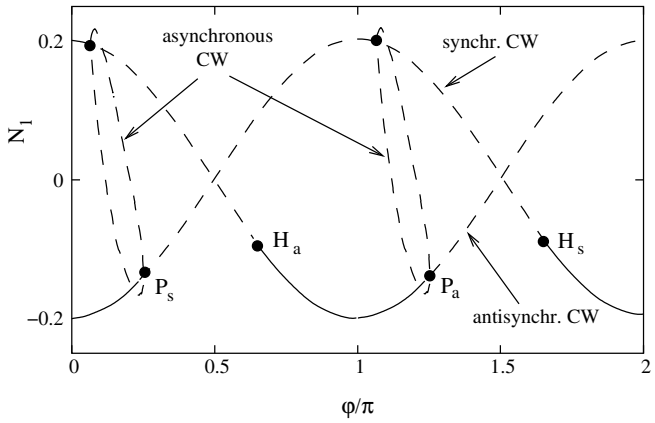

Figure 3: For fixed $\eta = 0.2$, there are two branches corresponding to the synchronous and antisynchronous solutions and the connecting branches of unstable asynchronous unstable periodic solutions. P_a and P_s are pitchfork and H_a, H_s are Hopf bifurcations. Index 's' stands for the synchronous and 'a' for antisynchronous solutions, respectively.

In the next section, we study system (3) for $\delta \neq 0$, i.e. we investigate the influence of the detuning.

6 Influence of the detuning

6.1 Preliminary study

Since system (3) has the phase-shift invariance property, we can reduce it to a 5-dimensional system. One way of reducing is to use the following transformation: $E_1(t) = a_1(t)e^{i\psi_1(t)}$, $E_2(t) = a_2(t)e^{i\psi_2(t)}$. Here a_1^2 and a_2^2 are intensities of the first and the second laser, respectively. We assume $a_1 \neq 0$ and $a_2 \neq 0$. $\Delta\psi = \psi_1 - \psi_2$ is their phase difference. Then with respect to the new real variables a_1, a_2, N_1, N_2, and $\Delta\psi$ we obtain the system of equations:

$$\begin{aligned} a_1' &= N_1 a_1 + \eta a_2 \cos(\Delta\psi + \varphi) \\ N_1' &= \varepsilon(J - N_1 - (N_1 + \nu)a_1^2), \\ a_2' &= N_2 a_2 + \eta a_1 \cos(\varphi - \Delta\psi), \\ N_2' &= \varepsilon(J - N_2 - (N_2 + \nu)a_2^2), \\ \Delta\psi' &= \delta + (N_1 - N_2)\alpha - \eta\frac{a_2}{a_1}\sin(\Delta\psi + \varphi) + \eta\frac{a_1}{a_2}\sin(\varphi - \Delta\psi). \end{aligned} \tag{8}$$

System (8) no longer posses the phase shift symmetry, and, therefore, all CW solutions become stationary states in terms of new variables.

Let us introduce the frequencies Ω_1 and Ω_2 by

$$\Omega_1(t) = \psi_1'(t), \quad \Omega_2(t) = \psi_2'(t).$$

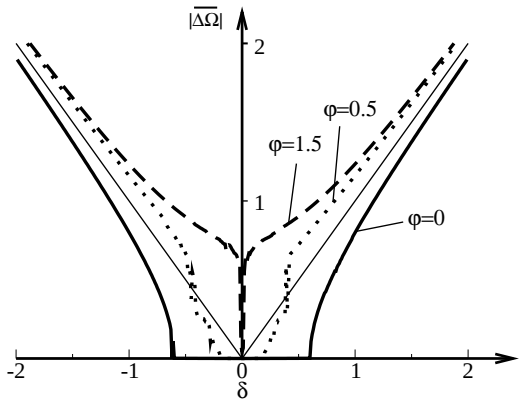

Figure 4: Averaged frequency difference versus detuning parameter for different values of φ ($\eta = 0.3$).

The following quantity determines the locking between two weakly coupled oscillators:

$$\overline{\Delta\Omega} = \langle \Delta\psi'(t) \rangle = \lim_{T\to\infty} \frac{1}{T} \int_0^T \Delta\psi'(t)dt = \lim_{T\to\infty} \frac{\Delta\psi(T)}{T}.$$

$\overline{\Delta\Omega}$ can be treated as averaged frequency difference between two weakly coupled lasers.

Figure 4 shows results of computation of $\overline{\Delta\Omega}$ depending on the detuning δ. Three different curves were obtained for different values of φ with fixed $\eta = 0.3$. At each point, we integrated over the transient interval $T_{\rm tr} = 1000$ and averaged over $T_{\rm av} = 1000$. Initial conditions were chosen at random. One clearly observes the locking intervals $\overline{\Delta\Omega} = 0$ as platoes near $\delta = 0$. Moreover, the width of these intervals strongly depend on the phase parameter φ. We will inspect the dependence of the locking on φ in more details in next sections by studying bifurcations that are involved in the loss of locking and appearance of pulsations. Additionally, we have to note that the use of frequency difference $\overline{\Delta\Omega}$ for investigating of the locking between two coupled oscillators can be justified in the case of weak coupling, i.e. small enough η. Therefore, we have to consider Fig. 4 as a preliminary result, which has to be accompanied by an additional bifurcation analysis in the next sections.

6.2 Stationary states for the case with detuning

The CW solutions of system (3) are equilibria of system (8). Hence, one can use the standard path-following technique to follow their dependence on the parameters. As starting data, we use the known stationary states for the symmetric system (see Fig, 3). The resulting bifurcation diagram is shown in Fig. 5, which is computed for the detuning $\delta = 0.1$. Before analyzing the obtained bifurcation diagrams, it is important to realize that detuning breaks two symmetries in our system (cf. Sec. 3): Z_2 symmetry $(E_1, N_1, E_2, N_2) \to$

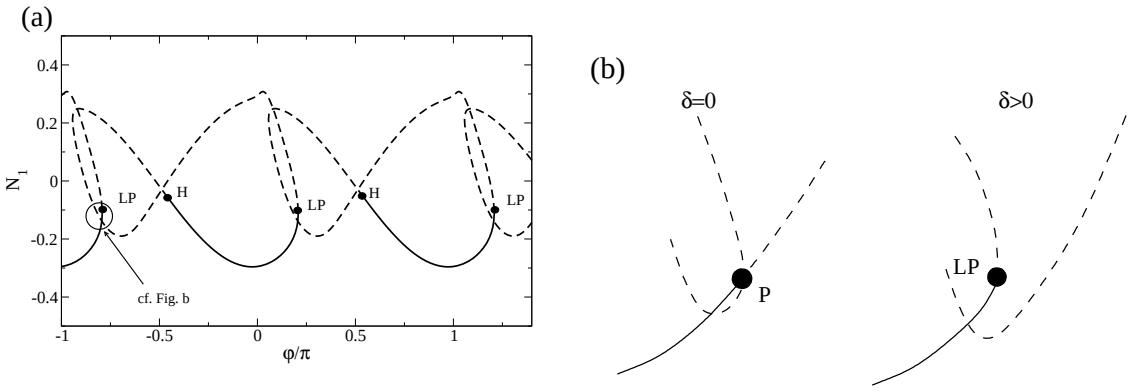

Figure 5: (a) Stationary states for system (3) with detuning. $\delta = 0.01$, $\eta = 0.2$. Stable branches are depicted by solid lines, unstable by dashed. (b) Perturbation of the pitchfork bifurcation by the detuning, zooming of some part of (a)

(E_2, N_2, E_1, N_1) and the symmetry $(E_1, N_1, E_2, N_2) \to (-E_2, N_2, E_1, N_1)$. Therefore, synchronous and antisynchronous solutions do not exist anymore. Moreover, the pitchfork bifurcations that partially determine the synchronization region of the system without detuning is no longer admissible for $\delta \neq 0$. Two questions arise naturally: What happens with the synchronous and antisynchronous solutions after the symmetry breaking by detuning? How is the pitchfork bifurcation perturbed in this case? The observed scenario, cf. Fig. 5, clarifies the situation. In particular, as can be seen from Fig. 5b, instead of the pitchfork bifurcation we have a saddle-node bifurcation (denoted as 'LP'). In the nonsymmetric case this saddle-node bifurcation connects the previously synchronous solutions via the unstable branch of asynchronous solutions to the antisynchronous, cf. Fig. 5a. Note that such a perturbation of the pitchfork bifurcation is common for symmetrically coupled systems with a parameter mismatch [19]. As a result, instead of the separate branches of synchronous and antisynchronous solutions, for $\delta \neq 0$ there are closed branches of solutions, which do not posses these symmetry properties. Nevertheless, as we shall see in Sec. 6.4, some parts of these branches still keep being close to the synchronous state and some to the antisynchronous.

Comparing the bifurcation diagram in Fig. 5 and its symmetric counterpart in Fig. 3 we note that similar stability regions for stationary states, which are limited by the Hopf (H) and saddle-node (LP) bifurcations, exist in both cases. In fact, they can be obtained from each other by continuation along the parameter δ. Moreover, as we will see in Sec. 6.4, the corresponding branches are close to the synchronous (those that contain $\varphi = 0$) and to the antisynchronous one (containing $\varphi = \pm 1$). It is evident that for these stationary states correspond to $\Delta\psi(t) = \text{const}$. In the following, by the locking between coupled systems with detuning (3) we understand the existence of the stable stationary states (for them we have $\Delta\psi = \text{const}$).

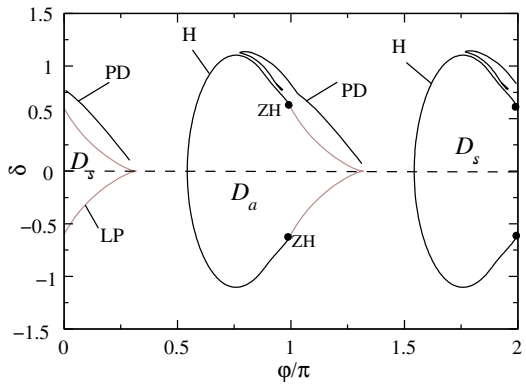

Figure 6: Stability regions for the stationary states of coupled systems with detuning. 'LP' and 'H' denotes saddle-node and Hopf bifurcations, respectively. 'ZH' is a codimension 2 Zero-Hopf (or Guckenheimer-Gavrilov) bifurcation point. 'PD' - period-doubling bifurcation curve for rotations of (8).

6.3 Regions of locking

The only parameter in our model, which induces mismatch between the lasers is the detuning δ. In order to study the influence of δ on stable frequency-locked states, we investigate the boundaries of the stability region, i.e. the bifurcation points 'LP' and 'H' in Fig. 5a, depending on δ. The resulting bifurcation diagram is shown in Fig. 6. There we denote by D_s and D_a two regions, corresponding to the existence of stable locked stationary states. We distinguish between these two regions because the first one is connected to the synchronous stationary states and the second one to the antisynchronous at $\delta = 0$. For more details about these states we refer to the next section. The Hopf bifurcation line is marked by black color and the saddle-node bifurcation by gray.

Note that the diagram in Fig. 6 is obtained for fixed coupling strength η. Another way of representation is to consider detuning δ and coupling strength η as the active parameters. Fig. 7 shows such bifurcation diagrams for fixed values of ϕ. The different values of ϕ correspond to qualitatively different bifurcation diagrams. The regions of stability of CW solutions are marked by gray color. As it is expected, for sufficiently small coupling η in Figs. 7a-7c, the stability region is bounded by saddle-node bifurcation lines. For $\phi = -0.84$ and $\phi = 1.41$, in addition to saddle-node bifurcation mechanism, Hopf bifurcation lines appear to confine partially the locking regions. The codimension two bifurcation points (ZH) appear where Hopf and saddle-node bifurcation lines meet.

The symmetry of the bifurcation diagrams in Figs. 6 and 7 with respect to interchange $\delta \to -\delta$ can be explained by the fact that system (3) is invariant under the following transformation $(E_1, E_2, N_1, N_2, \delta) \to (E_2 e^{i\delta t}, E_1 e^{i\delta t}, N_2, N_1, -\delta)$.

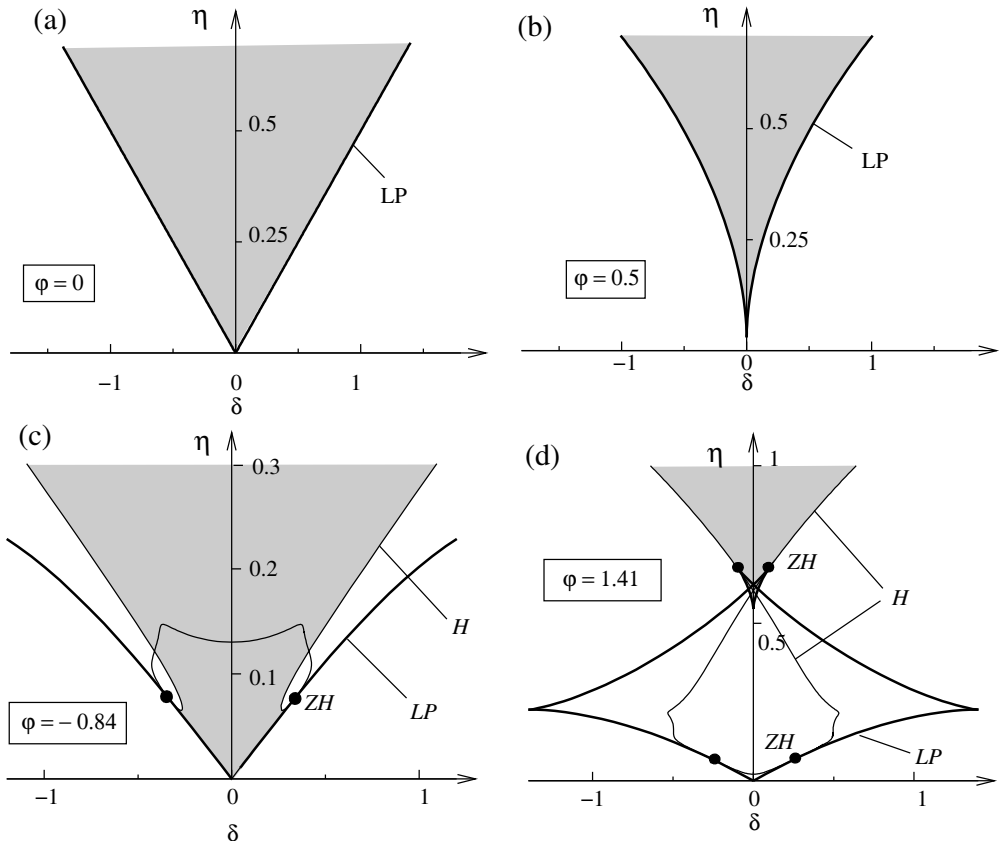

Figure 7: Bifurcation diagrams with respect to coupling strength η and detuning δ for fixed $\varphi = 0$ (a), $\varphi = 0.5$ (b), $\varphi = -0.84$, $\varphi = 1.41$. Hopf bifurcations (H) are denoted by thin lines and saddle-nodes (LP) by more heavy lines. Stability regions for stationary states are markey in gray. ZH are zero-Hopf (or Guckenheimer-Gavrilov) bifurcation points of codimension two.

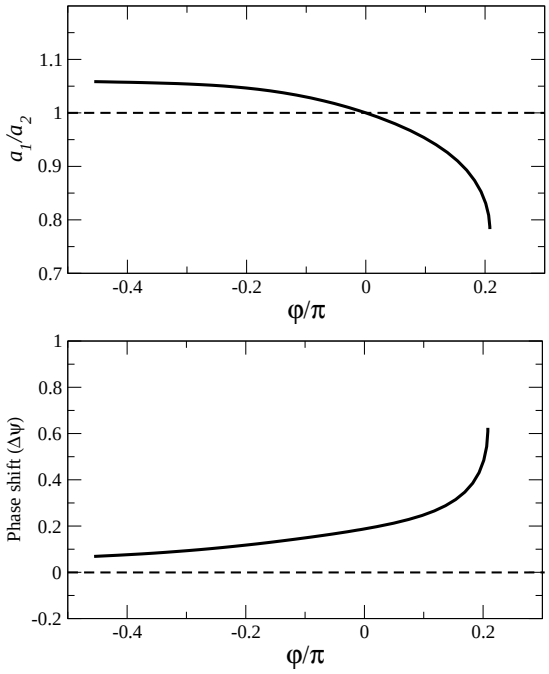

Figure 8: Characteristics of some locked solutions from the region D_s of Fig. 6.

6.4 Properties of the stationary states after the symmetry breaking.

By definition, CW solutions As we have seen in the previous section, the set of frequency-locked solutions consists of CW solutions of the form

$$E_1(t) = a_1 e^{i(\omega t + \Delta\psi)}, \quad E_2(t) = a_2 e^{i\omega t}, \quad N_1(t) = N_1 = \text{const}, \qquad N_2(t) = N_2 = \text{const}.$$

Now we show that their particular shape, i.e. the values of $a_1, a_2, \Delta\psi$, is influenced by the symmetry that is broken by the detuning δ. Particularly, in the region D_s (see Fig. 6) we have stationary solutions that are close in some sense to synchronous and in the region D_a close to antisynchronous states. This becomes clear when one note that the region D_s contains the set of synchronous states when $\delta = 0$ and D_a contains antisynchronous states. In other words, as $\delta \to 0$ the stable locked solutions from the region D_s continuously approach the synchronous CW states, and from D_a the antisynchronous, respectively. For the synchronous solutions one has $a_1/a_2 = 1$ and $\Delta\psi = 0$ and antisynchronous $a_1/a_2 = 1$ and $\Delta\psi = \pm\pi$. As an example, we plot in Fig. 8 the ratio of amplitudes a_1/a_2 and a phase-shift $\Delta\psi$ as a function of φ for $\delta = 0.2$, i.e. parameters belong to D_s.

6.5 Self-pulsations

Self-pulsations, i.e. periodic oscillations of the field intensity, appear as a result of the Hopf bifurcation of the stationary locked states. In terms of the original system (3) they are

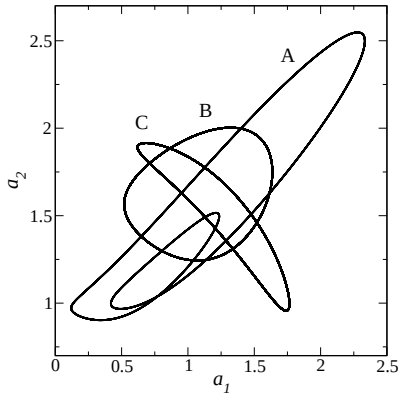

Figure 9: Different types of self-pulsations.

invariant tori, while for system (8) these solutions become either a periodic solutions, or rotations, which are periodic with respect to the variables a_1, a_2, N_1, N_2 but with unbounded variable $\Delta\psi$ such that $\Delta\psi(t+T) = \Delta\psi(t) + 2k\pi$ with some integer k. Such a solutions can be studied either directly by AUTO continuation software [20] or can be treated as bounded limit cycles after appropriate coordinate transformation, which allows to consider $\Delta\psi$ modulo 2π. Both approaches allows one to make bifurcation analysis of such solutions. In this way we detected a period-doubling bifurcation, which, together with a Hopf bifurcation of the stationary solutions, restrict the region where stable self-pulsations occur cf. Fig. 6.

It is also interesting to observe which shape of pulsations corresponds to different parameters. In particular, we have noticed, that near the period-doubling bifurcation self pulsations appear, which are close to the diagonal in the space (a_1, a_2), cf. Fig. 9, orbit A. On the contrary, near the Hopf bifurcation, we observe that self pulsations are close to the "antidiagonal". Such a phenomenon was reported in [14] and called "inverse synchronization". A more detailed analysis of it will be provided in a separate study.

6.6 Appearance of chaotic oscillations near Zero-Hopf bifurcation point

In the vicinity of the Zero-Hopf bifurcation point, cf. Fig. 10, there is a branch of Neimark-Sacker bifurcations emerging from ZH point (see general case in [21]). When crossing this curve from above, the stable limit cycle undergoes Neimark-Sacker bifurcation. It is a general observation (cf. [21], page 302) that the torus created by the Neimark-Sacker bifurcation exists only for parameter values near the corresponding bifurcation curve. If one moves away from the curve, the torus losses its smoothness and will be destroyed. The complete sequence of events is likely to involve an infinite number of bifurcations, since any weak resonance point on the Neimark-Sacker curve is the root of Arnold phase-locking tongue. In view of this fact, we did not try to resolve the bifurcations numerically below

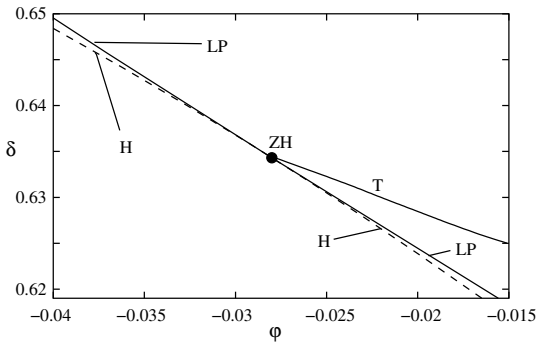

Figure 10: Unfolding of the Zero-Hopf bifurcation. 'T' denotes the Neimark-Sacker bifurcation curve emerging from the Zero-Hopf point.

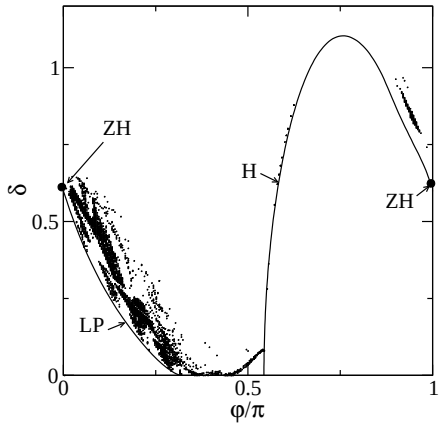

Figure 11: Parameter values, for which an attractor with positive largest Lyapunov exponent exists.

the curve 'T' in Fig. 10. Instead, for randomly chosen initial conditions, we calculated Lyapunov exponents for different parameter values. Figure 11 shows the parameter values for which the largest Lyapunov exponent is positive, i.e. the complex dynamics is present. We can see that, in particular, such region comes arbitrary close (with the given precision) to ZH point.

7 The case of a small delay

In this section we discuss some properties of the symmetric system with small delay

$$\begin{aligned} E_j'(t) &= (1+i\alpha)N_j(t)E_j(t) + \eta e^{-i\varphi}E_{3-j}(t-\tau), \\ N_j'(t) &= \varepsilon[J - N_j(t) - (N_j(t)+\nu)|E_j(t)|^2], \quad j = 1,2. \end{aligned} \tag{9}$$

and compare them with the corresponding properties of the instantaneously coupled system (4).

The dynamics of (9) within the synchronization subspace $E_1 = E_2 := E$, $N_1 = N_2 := N$ is governed by the Lang-Kobayashi equation [17]

$$\begin{aligned} E' &= (1 + i\alpha)NE + \eta e^{-i\varphi} E(t - \tau) \\ N' &= \varepsilon[J - N - (N + \nu)|E|^2]. \end{aligned} \tag{10}$$

The parameters of the synchronous CW solutions $E(t) = ae^{i\omega t}, N(t) = N = \text{const}$ of (10) satisfy the following set of equations (cf. [22, 23])

$$\begin{aligned} N &= -\eta \cos(\varphi + \omega\tau), \\ \omega - \alpha N &= -\eta \sin(\varphi + \omega\tau), \\ a^2 &= (J - N)/(N + \nu). \end{aligned} \tag{11}$$

One can obtain sufficient conditions for system (10) to have only one external cavity mode, i.e. a unique solution of (11). For this, we shall write the equation for ω as

$$\omega = -\eta(\alpha \cos(\varphi + \omega\tau) + \sin(\varphi + \omega\tau)). \tag{12}$$

The saddle-node bifurcation, which gives rise to additional external cavity modes, can be identified (cf. [22]) as a double root of (12). Hence, differentiating it with respect to ω, we obtain

$$1 = \tau\eta(\alpha \sin(\varphi + \omega\tau) - \cos(\varphi + \omega\tau)).$$

It is clear that the condition

$$\tau\eta < \frac{1}{\sqrt{1 + \alpha^2}} \tag{13}$$

guarantees that a double root does not exist. Hence, the inequality (13) roughly provides the limit within which one might expect that the delay τ does not qualitatively change the dynamics within the synchronization (antisynchronization) subspace.

The transverse stability of the unique synchronous CW solution is determined by the solutions of the characteristic equation

$$\begin{aligned} \chi_T^\tau(\Lambda) \;=\; & \left[\Lambda^2 + 2\eta\cos\theta(e^{-\Lambda\tau} + 1)\Lambda + \eta^2(e^{-\Lambda\tau} + 1)^2\right](\Lambda + \varepsilon(1 + S)) \\ & + 2\varepsilon S(\nu - \eta\cos\theta)\left[\Lambda + \eta(\cos\theta - \alpha\sin\theta)(e^{-\Lambda\tau} + 1)\right] = 0, \end{aligned} \tag{14}$$

where

$$S := \frac{J - \eta\cos\theta}{\nu + \eta\cos\theta}$$

and

$$\theta := \omega\tau + \varphi.$$

The derivation is given in Appendix A. The condition $\chi_T^\tau(0) = 0$ determines the pitchfork and $\chi_T^\tau(i\Omega) = 0$ Hopf bifurcation, respectively. It turns out that for the values up to $\tau = 2$ the regions in the (φ, δ) parameter plane for the transverse stability of synchronous CW solution of (9) are qualitatively the same as in the case of zero delay (4). In Fig. 12 we plot the curves which delineate this stability region. All the remaining parameters are taken to be the same as in Fig. 1. The effect of delay for this range of τ can be only seen by continuous changing of the slope of the curves.

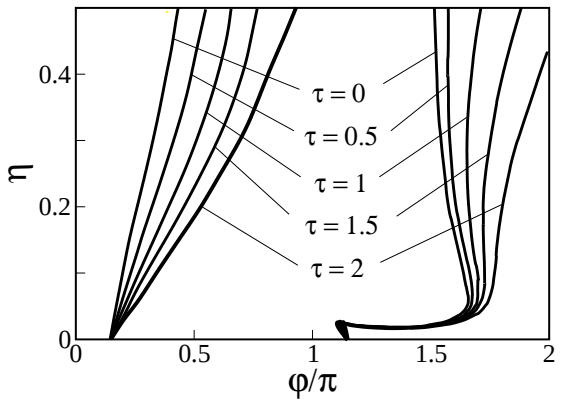

Figure 12: Boundaries of the region for transverse stability of synchronous CW solutions of system (9) for different values of delay. (similarly as in Fig. 1 without delay.) The corresponding boundaries for antisynchronous CW solutions can be obtained by shifting along the φ axis by π.

8 Conclusion

In this paper we studied a model for a single mode lasers which are optically coupled in a face to face configuration. The external cavity length is assumed to be short. We have derived conditions for the stability of synchronous CW solutions in terms of the coupling parameters. As a result of symmetry considerations, the properties of antisynchronous solutions can be determined by those of the synchronous. We have shown that when a detuning is present between two lasers, there exist stable stationary states under some parameter constellations, which can also be considered as a phase locked states with $\Delta\psi = \text{const}$. Moreover, the connection between these states and the synchronous solutions of the symmetric system (i.e. without detuning) is shown. We also investigate the mechanisms of appearance of self-pulsations, which are quasiperiodic solutions in terms of the original system (3) and represent periodic solutions of the reduced system (8). These mechanisms include Hopf bifurcation of the stationary phase-locked states and period-doubling bifurcation. We have shown that one of the organizing centers of chaotic pulsations in the considered system is a Zero-Hopf (or Guckenheimer-Gavrilov) codimension-2 bifurcation point. From the point of view of modeling, we studied the possibility to use the model (3) with instantaneous coupling for the study of coupled semiconductor lasers with short external cavity.

Acknowledgement
We wish to acknowledge useful discussions with Mathias Wolfrum, Hans-Jürgen Wünsche, and Nikolai Korneev. This work was supported by DFG (Sonderforschungsbereich 555 "Komplexe nichtlineare Prozesse").

A Derivation of the characteristic equations for synchronous solutions

The algorithm for the derivation of the characteristic equations for the synchronous CW solutions of systems (9) and (4) is the same, therefore, we present here the derivation in detail for the delayed system (9). Finally, the characteristic equation for (4) will be obtained by setting $\tau = 0$.

Let $E_1 = E_2 := E_s e^{\omega_s t}$, $N_1 = N_2 := N_s$ be the synchronous CW solutions under consideration. By $F_{1,2} = \frac{E_1 \pm E_2}{2} e^{-i\omega_s t}$ and $M_{1,2} = \frac{N_1 \pm N_2}{2}$ we introduce new coordinates such that (9) takes the form

$$\begin{aligned}
\dot{F}_{1,2}(t) &= (1+i\alpha)(M_1 F_{1,2}(t) + M_2 F_{2,1}(t)) - i\omega_s F_{1,2}(t) \pm \eta e^{-i(\varphi+\omega_s\tau)} F_{1,2}(t-\tau) \\
\dot{M}_1 &= \varepsilon(J - M_1 - (M_1+\nu)(|F_1|^2 + |F_2|^2) - M_2(F_1\bar{F}_2 + \bar{F}_1 F_2)) \\
\dot{M}_2 &= \varepsilon(-M_2 - (M_1+\nu)(F_1\bar{F}_2 + \bar{F}_1 F_2) - M_2(|F_1|^2 + |F_2|^2)).
\end{aligned} \tag{15}$$

F_1 and M_1 are the coordinates within the synchronization subspace, while the coordinates F_2 and M_2 are transversal to it [4, 18], i.e. we have $F_2 = 0$, $M_2 = 0$ for synchronized solutions.

System (15) is again autonomous due to the phase-shift invariance of the original system (9), and CW solution under consideration is transformed into the equilibrium $F_1 = E_s$, $M_1 = N_s$, $F_2 = 0$, $M_2 = 0$ with respect to it. We will linearize (15) in the vicinity of such point [24]. To perform this, we first decompose

$$F_{1,2} = x_{1,2} + iy_{1,2}.$$

Denoting with

$$\vec{v} := (v_1, \ldots, v_6)$$

variations in $x_1, y_1, M_1, x_2, y_2, M_2$, respectively, we obtain a linearization of the form

$$\frac{d}{dt}\vec{v}(t) = A\vec{v}(t) + B\vec{v}(t-\tau),$$

with the 6×6 matrices A and B having the block structure

$$A = \begin{pmatrix} A_1 & A_2 \\ A_2 & A_1 \end{pmatrix} \qquad B = \begin{pmatrix} B_1 & 0 \\ 0 & -B_1 \end{pmatrix}. \tag{16}$$

At a synchronized state, we have $x_2 = y_2 = M_2 = 0$ and $M_1 = N_{1,2} =: N$, and obtain

$$A_1 = \begin{pmatrix} N & \omega_s - \alpha N & x_1 - \alpha y_1 \\ -(\omega_s - \alpha N) & N & \alpha x_1 + y_1 \\ -2\varepsilon x_1(N+\nu) & -2\varepsilon y_1(N+\nu) & -\varepsilon(1 + x_1^2 + y_1^2) \end{pmatrix} \tag{17}$$

$$B_1 = \begin{pmatrix} \eta\cos(\varphi+\omega_s\tau) & \eta\sin(\varphi+\omega_s\tau) & 0 \\ -\eta\sin(\varphi+\omega_s\tau) & \eta\cos(\varphi+\omega_s\tau) & 0 \\ 0 & 0 & 0 \end{pmatrix} \tag{18}$$

The coupling terms in A_2 disappear for synchronized CW-states and the system splits into two invariant subspaces, corresponding to *synchronized* and *transverse* variations. As a consequence, the characteristic function can be factorized as $\chi^\tau(\Lambda) = \chi^\tau_L(\Lambda) \cdot \chi^\tau_T(\Lambda)$ with

$$\chi^\tau_L(\Lambda) = \det(\Lambda\,\mathrm{Id} - A_1 - e^{-\Lambda\tau} B_1) \tag{19}$$

and

$$\chi^\tau_T(\Lambda) = \det(\Lambda\,\mathrm{Id} - A_1 + e^{-\Lambda\tau} B_1). \tag{20}$$

Here Id is identical 3×3 matrix. The function χ^τ_L is the characteristic function of the Lang-Kobayashi system (10) and has been investigated in [22]. It determines the stability properties of the synchronous CW solution of coupled system (2). The function χ^τ_T determines its transverse stability properties. Taking into account equations (11), we can rewrite transverse characteristic equations in terms of the parameters in the form (14).

Similarly, the characteristic equations for the transverse stability of synchronous solution to (4) have the form (6).

B Set of equations for determining asynchronous CW solutions

Here we obtain a set of equations for determining asynchronous CW solutions of (4). We also present an algorithm of reducing it to a single nonlinear equation with one unknown variable $\psi \in [0, 2\pi]$.

After substituting (7) into (3), we obtain the following set of equations with respect to unknowns $a_1, a_2, \psi, \omega, N_1, N_2$

$$\begin{aligned} &a_1 i\omega = (1 + i\alpha) N_1 a_1 + \eta a_2 e^{-i(\psi+\varphi)}, \\ &a_2 i\omega = (1 + i\alpha) N_2 a_2 + \eta a_1 e^{i(\psi-\varphi)}, \\ &J - N_1 - (N_1 + \nu) a_1^2 = 0, \\ &J - N_2 - (N_2 + \nu) a_2^2 = 0. \end{aligned} \tag{21}$$

In real form it reads

$$a_1 N_1 + a_2 \eta \cos(\varphi + \psi) = 0, \tag{22}$$

$$a_1(\alpha N_1 - \omega) - a_2 \eta \sin(\varphi + \psi) = 0, \tag{23}$$

$$a_2 N_2 + a_1 \eta \cos(\psi - \varphi) = 0, \tag{24}$$

$$a_2(\alpha N_2 - \omega) + a_1 \eta \sin(\psi - \varphi) = 0, \tag{25}$$

$$J - N_1 - (N_1 + \nu) a_1^2 = 0, \tag{26}$$

$$J - N_2 - (N_2 + \nu) a_2^2 = 0. \tag{27}$$

Since $a_1 \neq 0$, we may set $x = a_2/a_1$. In the following we perform a formal procedure without checking signs and zeros of some functions, in order to avoid additional nonessential details.

As a result some spurious roots for new equation will appear which can be eliminated afterwards. The system for unknowns $x, \psi, \omega, N_1, N_2$ has the form

$$N_1 + x\eta\cos(\varphi+\psi) = 0, \tag{28}$$
$$(\alpha N_1 - \omega) - x\eta\sin(\varphi+\psi) = 0, \tag{29}$$
$$xN_2 + \eta\cos(\psi-\varphi) = 0, \tag{30}$$
$$x(\alpha N_2 - \omega) + \eta\sin(\psi-\varphi) = 0, \tag{31}$$
$$\frac{(J-N_2)(N_1+\nu)}{(J-N_1)(N_2+\nu)} = x^2, \tag{32}$$

where (32) is obtained from (26-27). Now we eliminate x from the following equations pairwise: (28-29), (30-31), (28-30), and (28-32). As a result we obtain equations for unknowns ψ, ω, N_1, N_2

$$N_1\sin(\varphi+\psi) + (\alpha N_1 - \omega)\cos(\varphi+\psi) = 0, \tag{33}$$
$$N_2\sin(\psi-\varphi) - (\alpha N_2 - \omega)\cos(\psi-\varphi) = 0, \tag{34}$$
$$N_1N_2 = \eta^2\cos(\varphi+\psi)\cos(\psi-\varphi), \tag{35}$$
$$\frac{(J-N_2)(N_1+\nu)}{(J-N_1)(N_2+\nu)} = \frac{N_1^2}{\eta^2\cos^2(\psi+\varphi)}. \tag{36}$$

N_1, N_2 can be determined using (33) and (34)

$$N_1 = \omega/(\alpha + \tan(\varphi+\psi)), \tag{37}$$
$$N_2 = \omega/(\alpha + \tan(\varphi-\psi)). \tag{38}$$

After substituting (37) and (38) into (35), ω can be expressed as a function of ψ:

$$\omega^2 = \eta^2\cos(\varphi+\psi)\cos(\varphi-\psi)(\tan(\varphi+\psi)+\alpha)(\tan(\varphi-\psi)+\alpha). \tag{39}$$

Final step is to substitute N_1 and N_2 from (37) and (38) into (36):

$$\frac{(J(\tan(\varphi+\psi)+\alpha)-\omega)\,(\nu(\tan(\varphi-\psi)+\alpha)+\omega)}{(J(\tan(\varphi-\psi)+\alpha)-\omega)\,(\nu(\tan(\varphi+\psi)+\alpha)+\omega)} = \frac{\eta^2}{\omega^2}\cos^2(\varphi+\psi)\,(\alpha+\tan(\varphi+\psi))^2 \tag{40}$$

After substituting (39) into (40), we arrive at a nonlinear transcendental equation for ψ. This equation can be treated numerically more easy since ψ is determined within a bounded interval $(0, 2\pi)$.

References

[1] G. D. VanWiggeren and R. Roy. Chaotic communication using time-delayed optical systems. *Int. J. Bifurcation Chaos Appl. Sci. Eng.*, 9:2129, 1999.

[2] Ingo Fischer, Yun Liu, and Peter Davis. Synchronization of chaotic semiconductor laser dynamics on subnanosecond time scales and its potential for chaos communication. *Phys. Rev. A*, 62:011801, 2000.

[3] M. Möhrle, B. Sartorius, S. Bauer, O. Brox, A. Sigmund, R. Steingrüber, M. Radziunas, and H.J. Wünsche. Detuned grating multisection-rw-dfb lasers for high-speed optical signal processing. *IEEE J. Selected Topics Quantum Electron.*, 7:217, 2001.

[4] L.M. Pecora, T.L. Carroll, G.A. Johnson, D.J. Mar, and J.F. Heagy. Fundamentals of synchronization in chaotic systems, concepts, and applications. *Chaos*, 7:520–543, 1997.

[5] J. Javaloyes, Paul Mandel, and D. Pieroux. Dynamical properties of lasers coupled face to face. *Phys. Rev. E*, 67:036201, 2003.

[6] A. Hohl, A. Gavrielides, T. Erneux, and V. Kovanis. Localized synchronization in two coupled nonidentical semiconductor lasers. *Phys. Rev. Lett.*, 78:4745–4748, 1997.

[7] Tilmann Heil, Ingo Fischer, Wolfgang Elsäßer, Josep Mulet, and Claudio R. Mirasso. Chaos synchronization and spontaneous symmetry-breaking in symmetrically delay-coupled semiconductor lasers. *Phys. Rev. Lett.*, 86:795, 2001.

[8] Michael Peil, Tilmann Heil, Ingo Fischer, and Wolfgang Elsäßer. Synchronization of chaotic semiconductor laser systems: a vectorial coupling-dependent scenario. *Phys. Rev. Lett.*, 88:174101, 2002.

[9] I. V. Koryukin and Paul Mandel. Two regimes of synchronization in unidirectionally coupled semiconductor lasers. *Phys. Rev. E*, 65:026201, 2002.

[10] C. Masoller. Anticipation in the synchronization of chaotic semiconductor lasers with optical feedback. *Phys. Rev. Lett.*, 86:2782, 2001.

[11] E. M. Shahverdiev, S. Sivaprakasam, and K. A. Shore. Parameter mismatches and perfect anticipating synchronization in bidirectionally coupled external cavity laser diodes. *Phys. Rev. E*, 66:017206, 2002.

[12] J. K. White, M. Matus, and J. V. Moloney. Achronal generalized synchronization in mutually coupled semiconductor lasers. *Phys. Rev. E*, 65:036229, 2002.

[13] S. Sivaprakasam, E. M. Shahverdiev, P. S. Spencer, and K. A. Shore. Experimental demonstration of anticipating synchronization in chaotic semiconductor lasers with optical feedback. *Phys. Rev. Lett.*, 87:154101, 2001.

[14] S.Sivaprakasam, Iestyn Pierce, Paul Rees, Paul S. Spencer, K. Alan Shore, and Angel Valle. Inverse synchronization in semiconductor laser diodes. *Phys. Rev. A*, 64:013805, 2001.

[15] Immo Wedekind and Urlich Parlitz. Synchronization and antisynchronization of chaotic power drop-outs and jump-ups of coupled semiconductor lasers. *Phys. Rev. E*, 66:026218, 2002.

[16] T. Heil, I. Fischer, W. Elsäßer, B. Krauskopf, K. Green, and A. Gavrielides. Delay dynamics of semiconductor lasers with short external cavities: Bifurcation scenarios and mechanisms. *Phys. Rev. E*, 67:066214, 2003.

[17] R. Lang and K. Kobayashi. *IEEE J. Quantum Electron.*, 16:347, 1980.

[18] S. Yanchuk, Yu. Maistrenko, and E. Mosekilde. Synchronization of time-continuous chaotic oscillators. *Chaos*, 13:388–400, 2003.

[19] S. Yanchuk, Yu. Maistrenko, and E. Mosekilde. Loss of synchronization in coupled Rössler systems. *Physica D*, 154:26–42, 2001.

[20] E.J. Doedel, H.B. Keller, and J.P. Kernévez. Numerical analysis and control of bifurcation problems: (I) Bifurcation in finite dimensions. *Int. J. Bifurcation Chaos Appl. Sci. Eng.*, 1:493–520, 1991.

[21] Yuri Kuznetsov. *Elements of applied bifurcation theory*, volume 112 of *Applied Mathematical Sciences*. Springer-Verlag, 1995.

[22] Matthias Wolfrum and Dmitry Turaev. *Opt. Commun.*, 212:127–138, 2002.

[23] G. H. M. van Tartwijk and G. P. Agarwal. *Prog. Quantum Electron.*, 22:43, 1998.

[24] J. K. Hale and S. M. Verduyn Lunel. *Introduction to Functional Differential Equations*, volume 99 of *Applied Mathematical Sciences*. Springer-Verlag, 1993.